SANDIA REPORT
SAND2011-7870
Unlimited Release
Printed October 2011

Dynamic Heat Capacity of the East Model and of a Bead-Spring Polymer Model

Jonathan R. Brown, John D. McCoy, and Douglas B. Adolf

Prepared by
Sandia National Laboratories
Albuquerque, New Mexico 87185 and Livermore, California 94550

Sandia National Laboratories is a multi-program laboratory managed and operated by Sandia Corporation, a wholly owned subsidiary of Lockheed Martin Corporation, for the U.S. Department of Energy's National Nuclear Security Administration under contract DE-AC04-94AL85000.

Issued by Sandia National Laboratories, operated for the United States Department of Energy by Sandia Corporation.

Available to DOE and DOE contractors from
U.S. Department of Energy
Office of Scientific and Technical Information
P.O. Box 62
Oak Ridge, TN 37831

Telephone: (865) 576-8401
Facsimile: (865) 576-5728
E-Mail: reports@adonis.osti.gov
Online ordering: http://www.osti.gov/bridge

Available to the public from
U.S. Department of Commerce
National Technical Information Service
5285 Port Royal Rd.
Springfield, VA 22161

Telephone: (800) 553-6847
Facsimile: (703) 605-6900
E-Mail: orders@ntis.fedworld.gov
Online order: http://www.ntis.gov/help/ordermethods.asp?loc=7-4-0#online

SAND2011-7870
Unlimited Release
Printed October 2011

Dynamic Heat Capacity of the East Model and of a Bead-Spring Polymer Model

Jonathan R. Brown and John D. McCoy
Department of Materials Science
New Mexico Institute of Mining and Technology
801 Leroy Place
Socorro, NM 87801

Douglas B. Adolf
Sandia National Laboratories
P.O. Box 5800
Albuquerque, New Mexico 87185

Abstract

In this report we have presented a brief review of the glass transition and one means of characterizing glassy materials: linear and nonlinear thermodynamic oscillatory experiments to extract the dynamic heat capacity. We have applied these methods to the east model (a variation of the Ising model for glass forming systems) and a simple polymeric system via molecular dynamics simulation, and our results match what is seen in experiment. For the east model, since the dynamics are so simple, a mathematical model is developed that matches the simulated dynamics. For the polymeric system, since the system is a simulation, we can instantaneously "quench" the system – removing all vibrational energy – to separate the vibrational dynamics from dynamics associated with particle rearrangements. This shows that the long-time glassy dynamics are due entirely to the particle rearrangements, i.e. basin jumping on the potential energy landscape. Finally, we present an extension of linear dynamic heat capacity to the nonlinear regime.

Contents

FIGURES

1.1. The Glass Transition

The primary physical phenomenon that this paper will discuss is the glass transition. Glass is a state of matter that for all practical purposes is a brittle solid, but does not have a crystal structure typical of other solids. Meaning that, dynamically, glasses are solids, but their structure is more similar to a disordered liquid. Glassiness is not tied to a particular substance or class of substances; many things that can form a solid of some sort can also form a glass if prepared correctly. For example, glasses can be formed from metals/alloys, polymers (i.e. rubbers, plastics, etc), and inorganic molecules (e.g. silica, the primary component of sand, is the main component in window glass). The glass transition is the transition, across timescales or thermodynamic quantities, between glassy, brittle behavior and rubbery, viscoelastic behavior. (see e.g. [1] for a recent review)

The dynamical nature of the transition is what makes glasses particularly hard to study. For it to be a "real" phase of matter, there would have to be a true thermodynamic phase transition between liquids and glasses (and there is good reason to think that this might be the case [2]). In this picture, the relaxation time diverges at a nonzero temperature T_0. On the other hand, the glass transition could be purely a dynamical phenomenon, and glasses are just supercooled liquids that can still flow, but just not on experimental timescales.

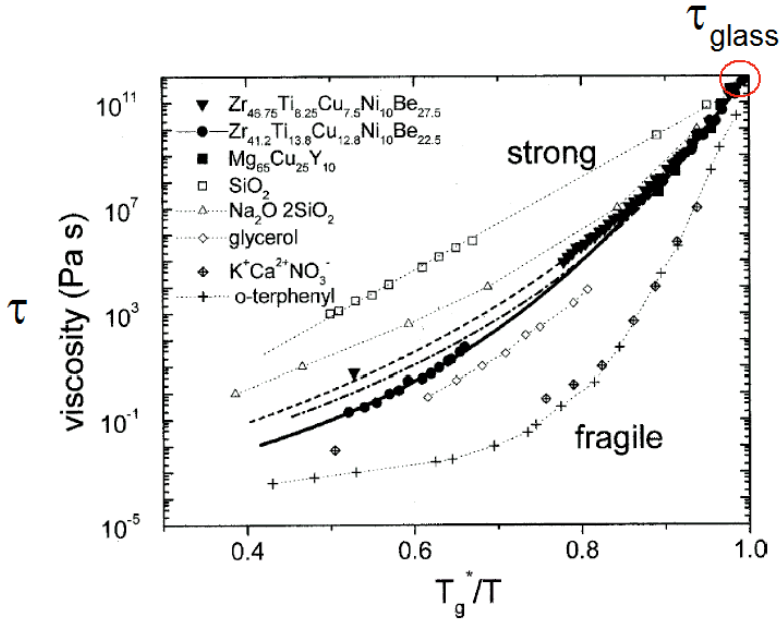

Figure 1. Angell plot for various substances. Viscosity (or approximately, relaxation time τ) is on the vertical axis on a logarithmic scale, and T_g/T is on the horizontal axis, where T_g is the temperature where the viscosity is 10^{12} Pascal-seconds. Therefore, the curve for each substance goes through the upper right hand corner. Strong glasses are ones that have straight lines on this sort of plot, all others are fragile. (image from [3])

A pragmatic approach is to define a "lab" glass transition time/viscosity where the time it takes to do an experiment outweighs the experimenter's patience (typically 10^{12} Pascal-seconds). This defines a lab glass transition temperature T_g, typically used in engineering applications. A standard visualization used in the study of glassy materials is an Angell plot, which plots relaxation time (on a logarithmic scale) against T_g/T (see Fig. 1) [3]. By construction, the curves for any material goes through the upper right hand corner, but they do not all approach it the same way. Strong glasses (such as window glass/silica) appear as a straight line (indicating an activated process), while fragile glasses have some curvature to them; that is, the relaxation time of fragile glasses increases very quickly as the system is cooled. That is, fragility in this context is a measure of how quickly the relaxation time (or equivalent) increases as the glass transition is approached.

1.2. Linear Response and Dynamic Heat Capacity

So far we have identified two interesting parameters to track to quantify glassy materials: the relaxation time and fragility. An experiment that is used to find these things is called a relaxation experiment. The dynamic heat capacity is a means to measure the relaxation behavior in the frequency domain.

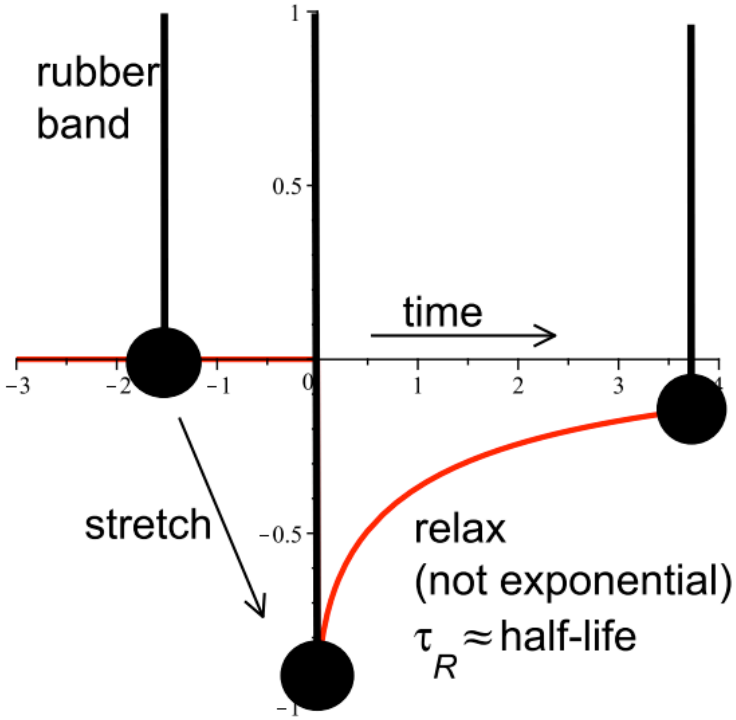

Figure 2. A schematic of the simple relaxation experiment described in the text.

An easily visualized example of a relaxation experiment is to hang a weight from the material you wish to test (such as a rubber band), let it come to equilibrium, slightly perturb it, release it, and record the response (diagrammed in Fig. 2) [4, 5]. The resulting relaxation curve then tells

you something about the relaxation time and fragility of the material. Counterintuitively, the relaxation function observed is not an exponential decay, but more closely follows a stretched exponential or Kohlrausch-Williams-Watts (KWW) function:

$$f(t) = f_0 \exp\left(-\left(\frac{t}{\tau}\right)^{\beta}\right) \qquad (1)$$

where τ is identified with the relaxation time, and β is a parameter between zero and one [6 , 7]. β is called the stretching parameter, and "spreads" the relaxation function over more timescales. Strong glasses, in general, have $\beta \approx 1$ and fragile glasses have $\beta < 1$; $\beta < 1$ also corresponds to a distribution of relaxation times.

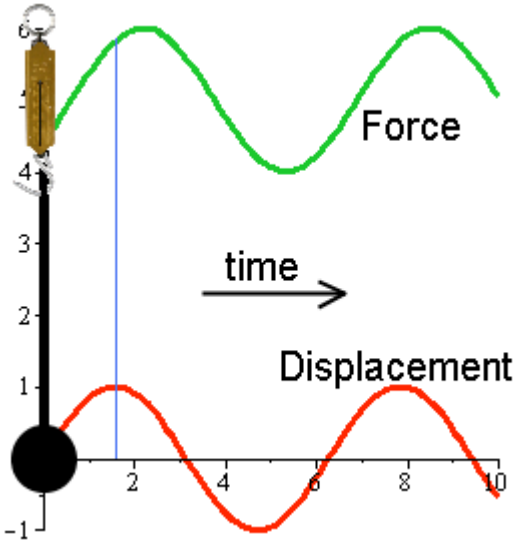

Figure 3. A schematic of the simple frequency domain relaxation experiment described in the text. The vertical line is a guide to the eye to show a phase lag between the two sinusoids.

We can also do a similar experiment in the frequency domain by driving the system's position sinusoidally (at an angular frequency ω) and watching the force (see Fig. 3). If the amplitude of the input sine wave is small, then the experiment in the linear response regime, and sine wave in gives us sine wave out. The ratio of input to output amplitudes and the amount of phase lag between the two defines a (complex valued) transfer function that is related to the time-domain relaxation function by a Fourier transform [8, 9, 10]. Since the Fourier transform is invertible, either representation contains the same information.

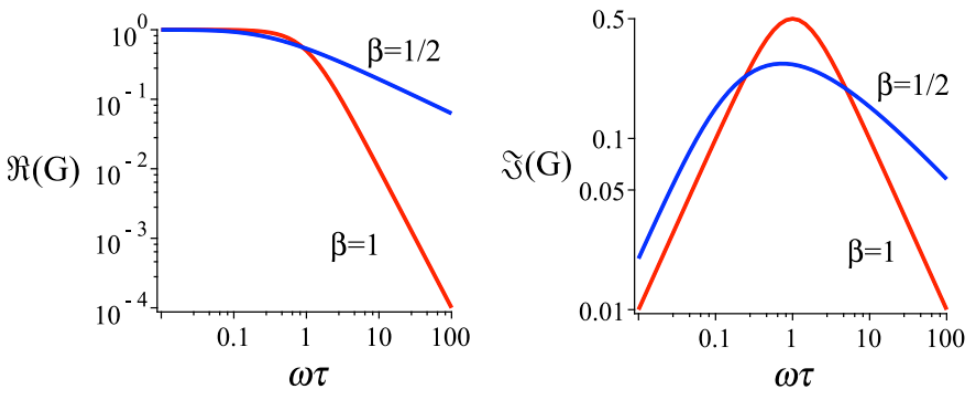

Figure 4. The real (left) and imaginary (right) parts of the KWW function in the frequency domain on with log-log scaling for two different value of β.

Relaxations functions in the frequency domain have the typical form shown in Fig. 4. A standard notation is to write the complex-values response function as $G(\omega) = G'(\omega) - iG''(\omega)$. The real part G' (or storage) represents the amount of response in phase with the forcing function (i.e. the elastic component) and plateaus at low frequencies where the system can keep up with the oscillations. Near the frequency corresponding to the relaxation time (i.e. $\omega\tau \approx 1$), the response starts to die off following a power law. The imaginary part G'' (or loss) is the out of phase component (i.e. the viscous component) and has a peak near the relaxation frequency (with power laws on either side). The stretching parameter β shows up as the power law exponent on the high frequency side of either component (see Fig. 4) so stretching in the time domain corresponds to an asymmetric peak in the frequency domain.

The KWW function does not have a simple analytic form in the frequency domain. Instead, a commonly used alternative is the Cole-Davidson (CD) function [11]:

$$G(\omega) \propto \frac{1}{(1+i\omega\tau)^{\beta}} \qquad (2)$$

where ω is angular frequency. The parameters τ and β play the same role in both functions, although the KWW parameters are not numerically equal to the CD parameters [9].

Both of these functions (CD and KWW) are empirical fits to observed data, but they seem to work across various types of relaxation experiments and materials.

A related experiment to the general example above is to vary the temperature sinusoidally and measure the energy (or visa-versa) [12, 13]. The frequency domain relaxation function in this case is the dynamic heat capacity $C_V(\omega)$. The imaginary part of the dynamic heat capacity is of particular thermodynamic interest because it can be shown that it is proportional to the entropy generated per cycle:

$$S_{gen/cyc} = -\int_{cycle} \frac{dQ/dt}{T}\,dt = \pi\left(\frac{\Delta T}{T_0}\right)^2 C_V'' \qquad (3)$$

where dQ/dt is the heat flow (in this case, the change in internal energy), ΔT is the amplitude of the temperature variation, and T_0 is the mean temperature [14 , 15].

2.1. Background

A simple model for a material that includes particle-particle interactions is the Ising model. This model was initially created in 1924 as a model of magnetization with interaction between particles. In one dimension, we have a line or loop of particle with spin (up or down) that interact ferromagnetically or antiferromagnetically. High and low energy states are defined by whether adjacent spins are aligned or antialigned [16]. It is notable because the statistical mechanics and thermodynamics of the model are exactly solvable in one and two dimensions, and there is a phase transition in two dimensions but none in one dimension [16, 17].

A generalization of the Ising model to add a time element so as to apply to glassy systems was put forth in the mid 1980s [18, 19, 20]. The east model, proposed later, is the simplest of such systems in terms of analysis, and its total relaxation time has been solved. These models have thermodynamics identical to the standard Ising model but with complex dynamics.

2.1.1. East Model

The east model and its close cousin, the Fredrickson-Andersen (FA) model are modified versions of the one dimensional Ising model to include glassy dynamics. The fundamental idea comes from a theory of the glass transition: from observations of molecular dynamics simulations, glassy systems are dynamically heterogeneous. Some regions of the system are slow or low energy and other regions are fast or high energy, and the fast regions (or defects) moving through the system is what is really driving the long-time macroscopic relaxation. The trouble is, there is no clear picture about what these defects fundamentally are.

The east and FA model approach is to look at it from another point of view: in Ising models, the defects are clear. In a ferromagnetic Ising model the spins ``like" to be aligned with each other. For low temperatures, one gets blocks of aligned spins (and not all are in the same direction due to thermal fluctuations). This gives us a clear definition of what a defect is in this case: the intersection between two different blocks. But now we have the opposite problem, the defects are well defined, but (unlike in molecular dynamics where we have $F=ma$) we do not have dynamics. So, we add dynamics back in with the simple idea of mobility near defects. That is, new defects can only appear near other defects, and old defects can only relax if they are next to another defect. Doing this symmetrically is the FA model, which gives strong glassy behavior, and asymmetrically is the east model (where defects can only travel to the right or east), which gives fragile glass behavior [18, 19, 21, 22]. This argument is summarized in Fig. 5.

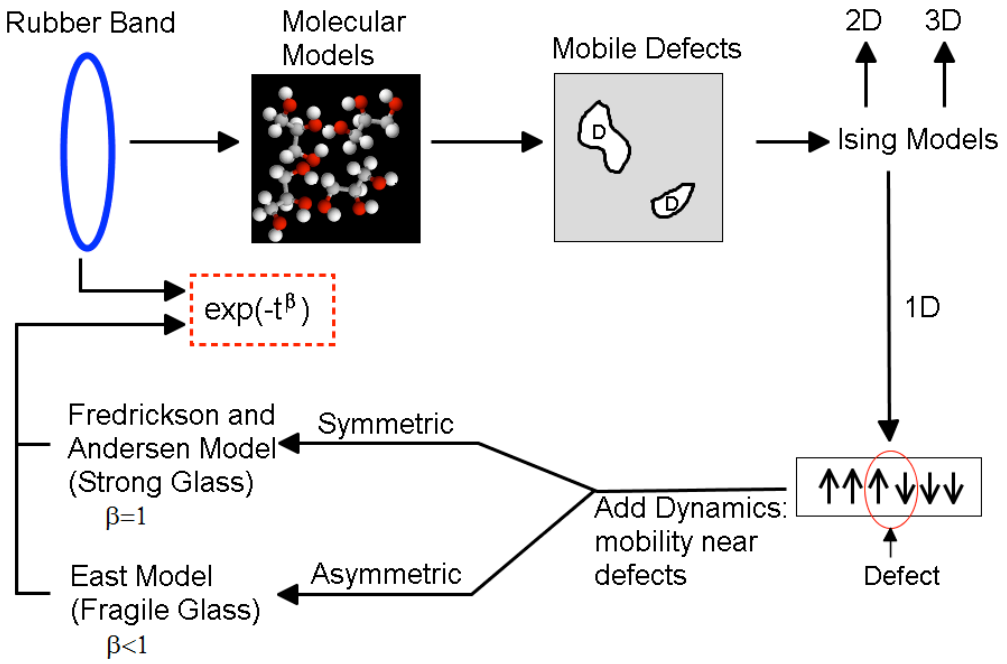

Figure 5. Flowchart of the justification of the east (and FA) model.

The east model has been widely studied in the glass community, and has a well established relation between the relaxation time and the temperature given by

$$\tau(T) = \tau_0 \exp\left(\frac{B}{T^2}\right) \tag{4}$$

where $1/(2\ln(2)) \leq B \leq 1/\ln(2)$ [23, 24]. Since $\log(\tau) \sim 1/T^2 \neq 1/T$, an Angell plot for the east model would have characteristically fragile curvature. But $\tau \to \infty$ only when $T \to 0$, so for the east model, we have fragile glass behavior arising without a divergence of relaxation time at nonzero temperature.

2.2. Methodology and Results

In this section, we present our work, published in the Journal of Chemical Physics (JCP) [25]. First, we ran simulations on the east model with an oscillating temperature, to extract the dynamic heat capacity, then we derived a mathematical model based on the rules of the east model to explain the dynamics we observed.

2.2.1. Simulation

Since the east model acts on the defects in the standard Ising model, we reformulate in terms of the "bonds" (or interfaces between the spins) alone. For example, instead of

↓↓↓↑↑↑↑↑↓↓↓↓↑↓↓

we write

00100001000110

The high energy sites are the defects (represented now as 1's), so we can write the nondimensionalized energy as

$$E = \sum_{i=1}^{N} s_i \tag{5}$$

where s_i (= 0 or 1) is the energy of each interface. By the definition of the east model, defects can only "move" to the right, so a defect can "flip" its right hand side neighbor up with nonzero probability that depends on temperature. For this we use a Boltzmann factor to set this probability, in order to keep the right thermodynamics. That is, set

$$\begin{aligned} P(10 \rightarrow 11) &= \exp(-1/T) \\ P(11 \rightarrow 10) &= 1 \\ P(00 \rightarrow 01) &= 0 \\ P(01 \rightarrow 00) &= 0 \end{aligned} \tag{6}$$

where T is the nondimensionalized temperature (i.e. we have set k_B=1). This allows us to run a Monte Carlo simulation on the model, where the system is some large string of 1's and 0's and time is advanced by the rules above.

As mentioned above, the transfer function between temperature and energy is the dynamic heat capacity. So, to measure it for a specific frequency ω, we set

$$T(t) = T_0 + \Delta T \sin(\omega t) \tag{7}$$

then, so long as ΔT is small compared to T_0 (we used $\Delta T = 0.05\ T_0$), we are in the linear response regime, and the measured energy E approximately follows

$$E(t) = E_0 + \Delta E(\omega) \sin(\omega t - \delta(\omega)) \tag{8}$$

where the symbols have a similar meaning as in the previous equation but also have a frequency dependence to them. The heat capacity is just the ratio of the amplitudes of these waves, but the addition of a phase lag between the two introduces an imaginary part. Explicitly,

$$C_V(\omega) = \frac{\Delta E(\omega)}{\Delta T}\left(\cos(\delta(\omega)) + i \sin(\delta(\omega))\right) \tag{9}$$

This procedure with sample output is shown in Fig. 6. Note the asymmetric shape of the imaginary peak indicates stretched exponential fragile dynamics.

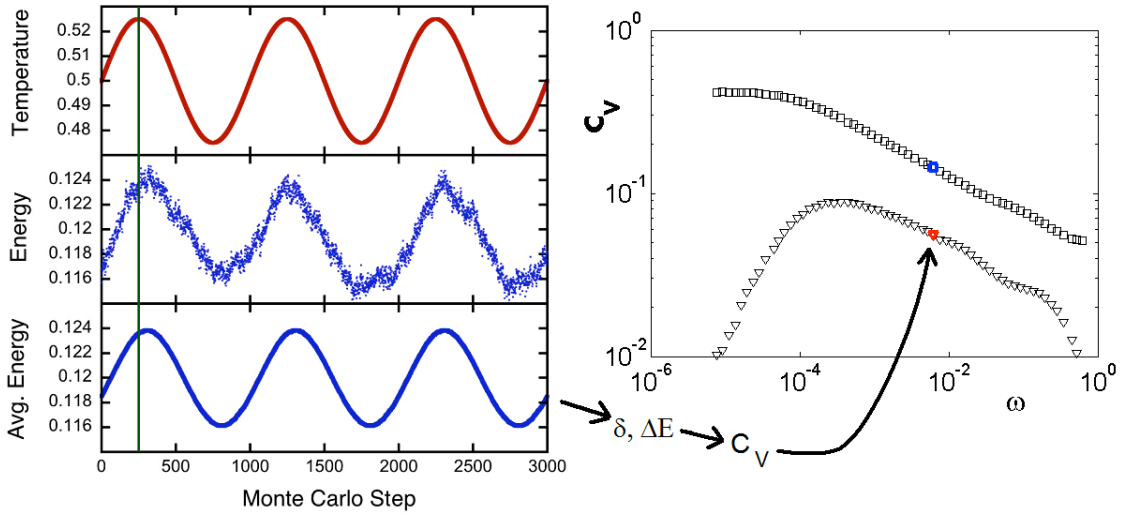

Figure 6. An example of the simulation procedure to calculate the dynamic heat capacity. On the left are time series of the temperature, energy, and average (in the sense that measurements spaced by the period of oscillation are averaged) energy of the Monte Carlo simulations. From this we fit a sinusoid to the average energy to derive the amplitude ΔE and phase lag δ, and we compute the heat capacity C_V by equation (9). This gives us a single point on the dynamic heat capacity spectrum (shown on the right). The squares are the real part and the inverted triangles are the imaginary part.

This procedure was run for a range of 39 temperatures between 0.2 and 10, and for each temperature, runs for logarithmically spaced (twelve per order of magnitude) periods of 10 to at most 10^9 were done as needed. The relaxation time was extracted with a curve fit and the results are shown in Fig. 7. Our results are consistent with theory, equation (4).

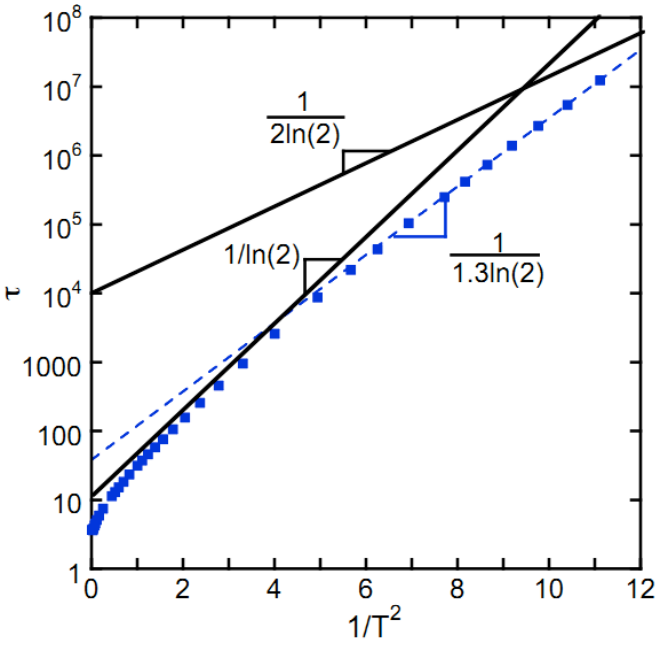

Figure 7. Plot showing the fit relaxation time (in Monte Carlo timesteps) plotted against $1/T^2$. On this sort of plot, equation (4) would appear as a straight line. The limits on the slope B are shown for comparison. The dashed line is a least squares fit.

2.2.2. Mathematical Model

Our mathematical model for the dynamics of the east model is based on the work of Sollich and Evans [26]. Basically, because we are interested in the low temperature dynamics of the system, we expect that the defects will be rare. So, we divide the system into "domains" of 0's terminated by a 1:

$$110000101000101 \rightarrow 1|1|00001|01|0001|01$$

Now, since the defects are rare at low temperature, we assume that the domains are isolated from each other, so we can solve for their dynamics independently. We can solve for the dynamics exactly using Markov chains [27]. In short, we derive a Markov chain that related the transitions between the allowed states of a domain from the rules of the east model, then calculate the mean first passage time to relax the far right spin. This then gives us a distribution of relaxation times that can transformed into a dynamic heat capacity spectrum.

While this procedure captures the high frequency/short time dynamics, where the domains are approximately isolated, it does not correctly model the long time dynamics. To correct this, we introduce a cutoff domain length $d_{\max}$ (a fitting parameter) after which the dynamics change to the nonisolated limit. In this region, domains are large and necessarily nonisolated, so it is far more likely that the 1 to the left of the domain will be relaxed before the domain relaxes on its own. In this case, the domain is effectively shrunk because the terminating left spin has been moved right (since it is likely that some of the inner 0's have been flipped up). Effectively, in the nonisolated limit, a domain relaxes at a rate proportional to its size. The results of the Markov chain analysis, with and without the nonisolated limit correction, are shown in Fig. 8.

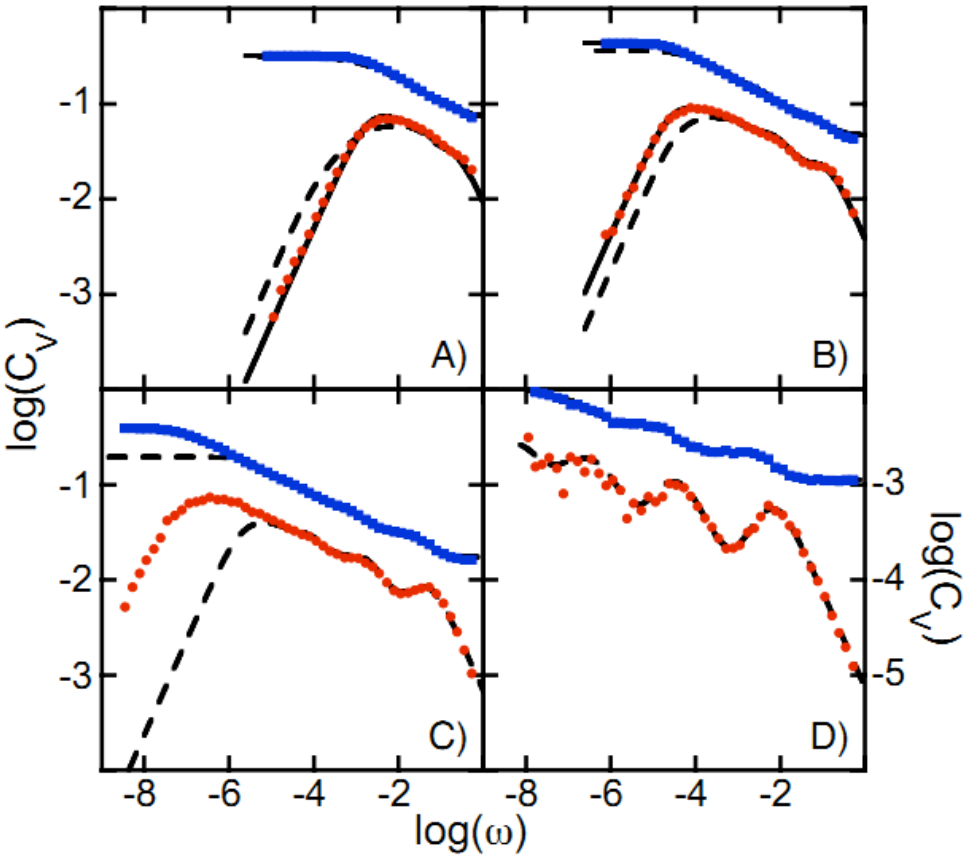

Figure 8. Real and imaginary components of the dynamic heat capacity plotted against frequency on a log-log scale for a range of temperatures. The squares and circles are the real and imaginary part of the simulation data, respectively, with every other point dropped for clarity. The dashed lines are the Markov chain computations, truncated by the number of terms that could be computed numerically. The solid lines are the corrected Markov chain model fit with a maximum isolated domain length d_{max} (see text). The parameters for the four plots are: A) a temperature of T=0.7, domain length at truncation d_{trunc}=20, and best fit maximum isolated domain length d_{max}=6; B) T=0.45, d_{trunc}=17, and d_{max}=14; C) T=0.32, d_{trunc}=16, and no possible fit for d_{max}; and D) T = 0.2, d_{trunc}=14, and no possible fit for d_{max}.

3. SIMPLE POLYMER MODEL

3.1. Bead Spring Model

The glassy model used in this section is a Newtonian molecular dynamics (MD) bead spring polymer model. Newtonian molecular dynamics is a simulation method on the atomistic scale, where Newton's second law is integrated numerically for some chosen interparticle and external potentials. The MD software we used was LAMMPS, an open source code from Sandia National Laboratory, which uses the velocity Verlet algorithm for the integration [28].

The specific model that we are using is a bead-spring polymer model, as in previous equilibrium work [29, 30, 31, 32, 33, 34]. This is a coarse grained model, in that the chemical details of the monomers are ignored; instead, the polymer chains are simply chains of single atom monomers (the beads) chained together with unbreakable bonds (the springs). This is not intended to model any specific real world polymer. Instead, the competing length scales of the bonds and the nonbonded interactions keep the system amorphous, and it therefore makes a good generic model for glassy polymers.

More specifically, the system used in this work had 80 ten-site chains and 5 single-site penetrants. The interactions between the particles are given by the Lennard-Jones (LJ) 6-12 interaction potential [35]:

$$U_{LJ}(r) = 4\varepsilon\left[\left(\frac{\sigma}{r}\right)^{12} - \left(\frac{\sigma}{r}\right)^{6}\right] \tag{10}$$

where r is the distance between molecules, and ε and σ are scaling factors in terms of energy and distance, respectively. The LJ 6-12 potential is a standard form for the interaction between two neutral particles. For short distances, the r^{-12} term dominates, and there is a strong repulsion resulting from the overlapping of electron clouds. For longer distances, the r^{-6} term dominates and describes the attractive behavior from Van der Waals forces. In our simulations, the system was nondimensionalized by setting ε, σ, the Boltzmann constant, and each particle's mass to one. That is, the units for the system are set to LJ units.

Although the LJ potential is defined for interactions at any distance, in practice it is far more computationally efficient to cut off the range of the potential at some finite distance r_c. To make the potential energy continuous, it's shifted so that at the cutoff distance the potential is zero.

Following Weeks, Chandler, and Andersen [36], the LJ potential can be decomposed into an attractive and repulsive part. The minimum value is easily computed to be at $r_c=2^{1/6}$, and cutting off the potential at that distance leads to a purely repulsive system. For the complete attractive and repulsive system (henceforth simply called attractive systems), we use $r_c=2*2^{1/6}$ for the cutoff. The short range of the interactions in the repulsive systems makes them very efficient in simulation. The repulsive system still models the excluded volume and repulsions between particles, and they have the same structure as the attractive systems [36]. However, the attractive

systems are more realistic, especially if one is interested in the internal energy and thermodynamics of the system. Because of the similar structure, the systems can be compared using packing fraction (the fraction of filled space, denoted by η) as a scalar metric [31]. Packing fraction remains a collapsing function in the present work as well; i.e. for a given system type (freely-jointed or freely rotating, see below) dynamical quantities, such as relaxation time, for various state points (temperatures, volumes, pressures) all fall on the same curve when plotted against packing fraction.

The bonds between atoms in a chain were simulated by also adding a standard model, the finite extensible nonlinear elastic (FENE) potential introduced by Kremer and Grest [37, 38, 39], which is given by

$$U_{FENE}(R) = \begin{cases} -0.5KR_0^2 \ln\left(1 - \left(r/R_0\right)^2\right) & r < R_0 \\ \infty & r > R_0 \end{cases} \tag{11}$$

For our simulations, we used values of K=30 and R_0=1.5. The choice of these parameters for this potential prevents crystallization because of the differing length scales to the standalone LJ potential [29].

In addition to the interparticle potentials, some of our systems also included a potential to fix the angle defined by three atoms on the backbone of the chains. In such systems, referred to as freely rotating (FR) systems, the angle is constrained by an additional harmonic potential:

$$U(\theta) = C\left(\theta - \theta_0\right)^2 \tag{12}$$

We used parameters K=500 and θ_0=120° to fix the backbone angle to 120 degrees. The systems without such a constraint are called freely jointed (FJ) systems. The extra constraint in the FR systems has the effect of stiffening the chains compared to the FJ system.

3.2. Linear Dynamic Heat Capacity

Similar to the east model, in order to extract the dynamic heat capacity, we took previously used equilibrated systems and subjected them to a sinusoidal temperature producing a sinusoidal (but lagged) energy; see equations (6), (7), and (8). For this model we used $\Delta T=0.1\ T_0$ for the linear response regime amplitude.

For each state point of the system (where we vary temperature, density, attractive vs. repulsive, and FJ vs. FR), each simulation only give the dynamic heat capacity at a particular frequency. So, in order to see the full dynamics for each system, we run 50-100 simulations to cover 5-8 orders of magnitude of frequencies with the frequencies spaced roughly equally apart on a logarithmic scale.

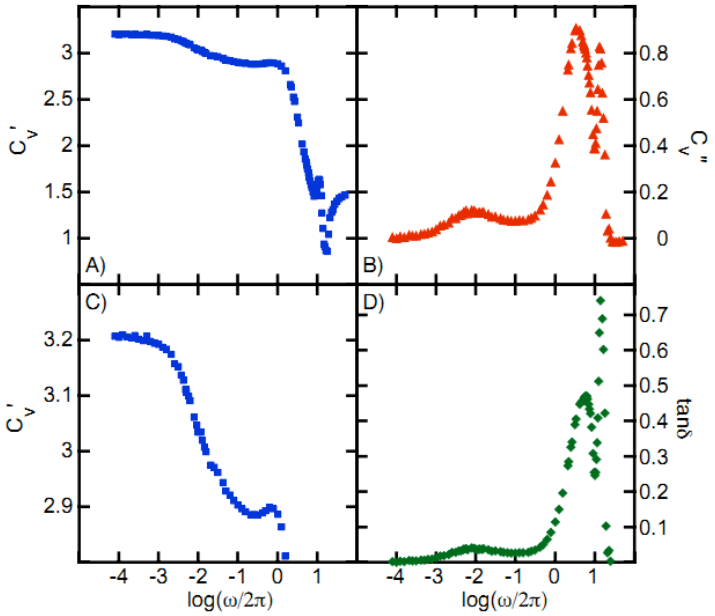

Figure 9. An example dynamic heat capacity spectra, where (a) storage, (b) loss, (c) zoomed in storage, and (d) tan(δ) are plotted against the logarithm of the frequency. The system pictured is an attractive FJ system with temperature T=0.6, density ρ=1.033, and packing fraction η=0.618.

See Fig. 9 for an example dynamic heat capacity spectra. The main difference from the general background above is that there are multiple distinct relaxation processes going on, resulting in two peaks in the imaginary part, and multiple plateaus in the real part. The low frequency peak (called the α-peak), which is only distinct at high packing fraction (see Fig. 10), corresponds to the system rearranging itself and is usually the relaxation time of interest. In fact, when a similar method is applied in experiment, only the α-peak behavior is visible because of physical limitations of the machinery involved, and our results are consistent to what is seen in experiment (see e.g Fig. 2 of [12]). As mentioned in section 1.2, the location of the α-peak (which is proportional to the inverse relaxation time) is only a function of the packing fraction for a given system type (FJ or FR). The higher frequency peaks (confusingly called β-peaks) correspond to thermal vibrations of the system; the peaks stay at about the same frequency, which roughly correspond to nonbonded/bonded particle-particle collision times, for all packing fractions.

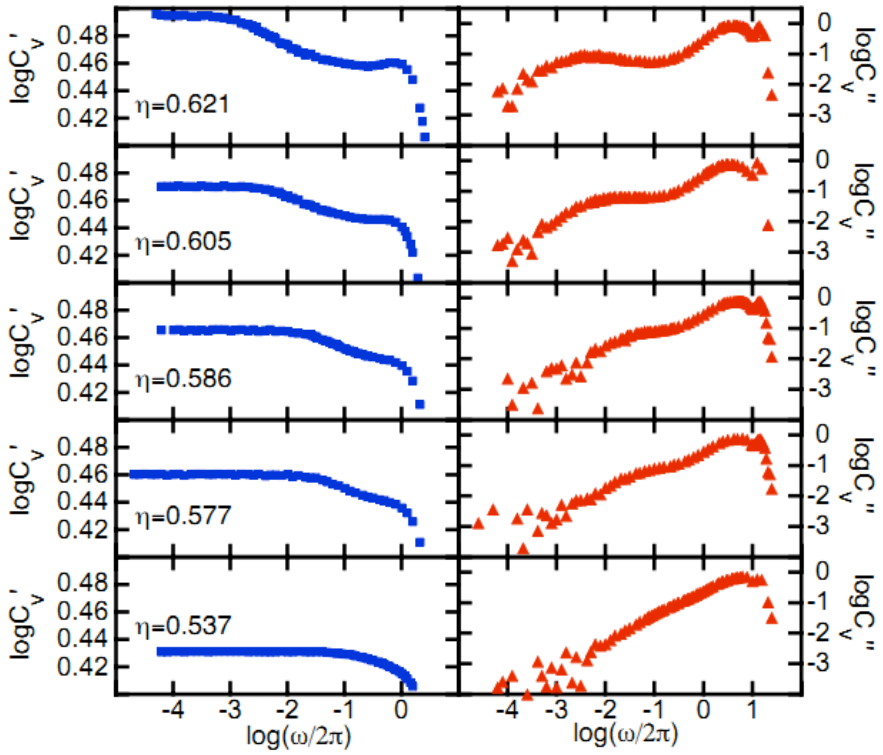

Figure 10. Example dynamic heat capacity spectra, where storage (left) and loss (right) are plotted against the frequency with log-log scaling. The systems used are repulsive FJ systems with the shown packing fractions.

For the FJ systems, 42 such frequency sweeps have been done (24 attractive 18 repulsive), and for the FR systems 36 have been done (all attractive).

A paper on the above results has been published in the Journal of Chemical Physics (JCP) [14].

3.3. Quenched Dynamic Heat Capacity

3.3.1. Background

A popular framework that is often used to explain the slowing of the dynamics in supercooled liquids is the potential energy landscape (PEL). In this picture, the entire system of N particles is treated as a single point in $3N$ dimensional space, and the dynamics are the natural extension of Newton's laws in this higher dimensional space. Namely the system feels a force in the downhill V direction, where V is the total system potential energy function. Thus, V defines a surface in $3N+1$ dimensional space that contains all of the dynamics of the system. In order to separate vibrations (the short-time dynamics), the local potential energy minimum of the system is found by "quenching". That is, $3N$ dimensional space is partitioned into equivalence classes of local minima (or basins) of the potential energy, where the local minima are interpreted as the inherent structure (IS) of the system and the "draining basin" around it is related to the vibrational motion [40]. These inherent structures are analogous to the crystal structure underlying atom locations in crystalline materials, where the atoms are not perfectly on the ideal locations of the crystal

structure but instead vibrate around those locations with thermal motion. The case is similar for the inherent structures in glasses, but these structures are amorphous instead of ordered.

Quenching in this context is a method in simulation where the vibrational energy (kinetic and potential) is completely and instantaneously removed. To do this, snapshots of the particle positions are saved periodically from a MD simulation. Using each snapshot as initial conditions of an optimization procedure, the system is allowed to "roll down" the PEL to the bottom of a local minimum, the IS. This is done by ignoring Newtonian dynamics, and instead using the particle positions as the variables and the energy as the objective function in an iterative optimization procedure. Provided that the barriers between IS are large compared to the energy of the system (which is the case at low temperature), this procedure will almost always produce the IS of interest.

The method of quenching simulations to probe the potential energy landscape was pioneered by Stillinger and Weber [40]. Their system was of monodisperse harmonically interacting particles, which have a phase transition into a crystal state. The quenched states of the system are crystals for all initial temperatures with dislocations and grain boundaries. The picture for glass forming liquids is less clear; both the quenched and unquenched states appear liquid-like in their structure. However, work by Schrøder et. al [41] showed that the dynamics of a binary Lennard-Jones system (a well known glass former) could be split into vibrational and inherent structure components by comparing the structural correlation function for the system with and without quenching.

From the PEL perspective, the distribution of relaxation times is the distribution of times required for the system to jump between different metabasins weighted by the energy difference [42, 43, 44]. This interpretation is explored in several recent studies where the PEL is simplified to a (scale-free) network with the nodes being inherent states and the edges being the energy barriers between them (and hence the probability per timestep of the system moving between nodes) [42, 45, 46]. The average relaxation time from this analysis matches the total relaxation time of the system from different measures (such as the diffusion coefficient [43, 44]). This interpretation naturally yields a distribution of relaxation times arising from a distribution of energy barrier heights and hence a distribution of mean waiting times to make a jump between nodes.

3.3.2. Methodology and Results

By directly tracking the energy response through the dynamic heat capacity, the dynamics of our model were split between a long time (low frequency) PEL contribution and a short time (high frequency) vibrational contribution. Our conclusions are similar to those of Schrøder et. al [41]. However, our frequency domain analysis provides a more direct argument for attributing the α-peak behavior to the dynamic response of the PEL.

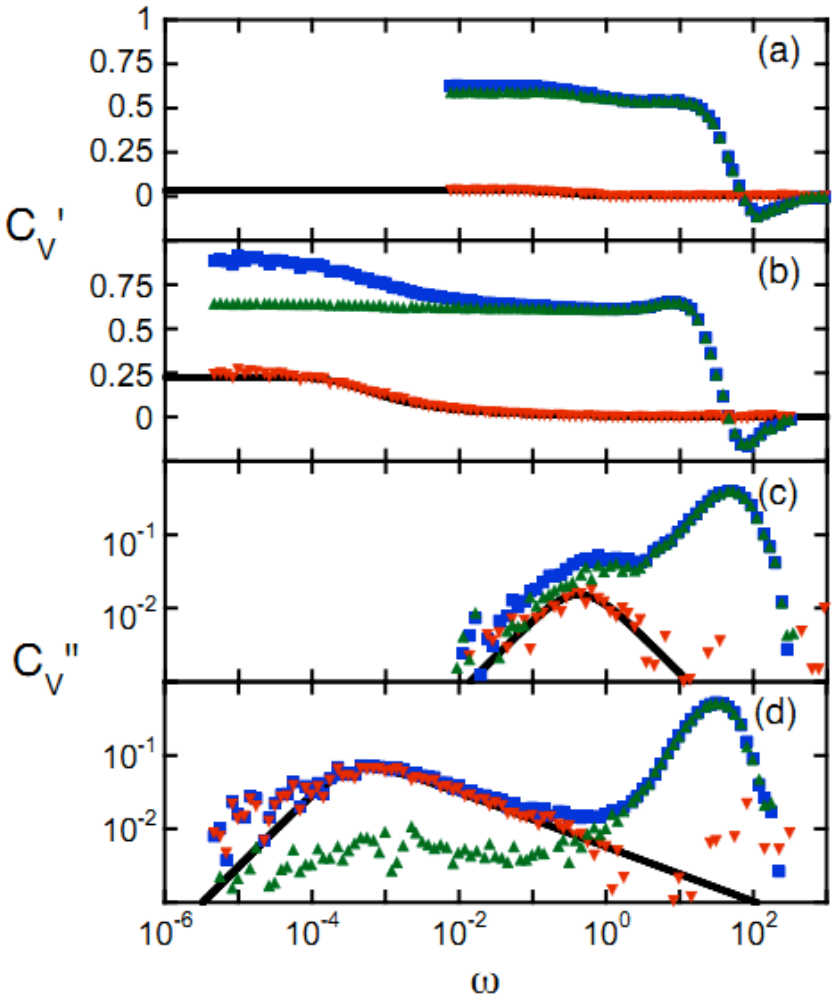

Figure 11. Plot of the nonbonded potential energy contribution to the dynamic heat capacity as a function of log frequency. Only the nonbonded contribution to the energy is of interest because the kinetic energy is a purely in phase contribution, and the contribution from the bonds has (nearly) no α-peak. a) The real part on a linear vertical scale for a low packing fraction system (T=4.0, ρ=1.033, η=0.481). The squares are the full heat capacity, the inverted triangles are the results from the quenching simulations, and the triangles are the difference between the two. The solid line is a least squares fit to a Cole-Davidson function. b) The real part on a liner vertical scale for a high packing fraction system (T=1.4, ρ=1.033, η=0.559). c) The imaginary part on a logarithmic vertical scale for the same low packing fraction system as in part (a). d) The imaginary part on a logarithmic vertical scale for the same low packing fraction system as in part (b). All symbols have the same meaning as in part (a).

In order to access the dynamics of the underlying inherent structures, we took a time series of snapshots of the system from the above dynamic heat capacity simulations and quenched them, as described above. In particular, we used the energy minimization routine in LAMMPS to perform the quenches, which uses a conjugate gradient algorithm or a Hessian-free quasi-Newton method (which we have switched to due to a recent software update) for the minimization. These quenches were performed at least four times per period (modulo the

period) and averaged over as many snapshots that could be computed in a reasonable amount of time, which were typically a few thousand snapshots per frequency. For very low frequencies, quenches were performed many times per period, but for most frequencies, many samples were averaged at four or eight points along the period of the oscillation.

The heat capacity computed from this procedure is the configurational or quenched heat capacity and is computed in exactly the same way as the standard dynamic heat capacity with the energy of the IS being used in place of the true energy.

The primary result of this procedure is that the α-peak remains largely unchanged in the quenched dynamic heat capacity, but the β-peaks are completely removed (see Fig. 11). This confirms the idea that long time relaxation is due to motion on the PEL; specifically, the particles rearranging themselves by moving from one IS to another.

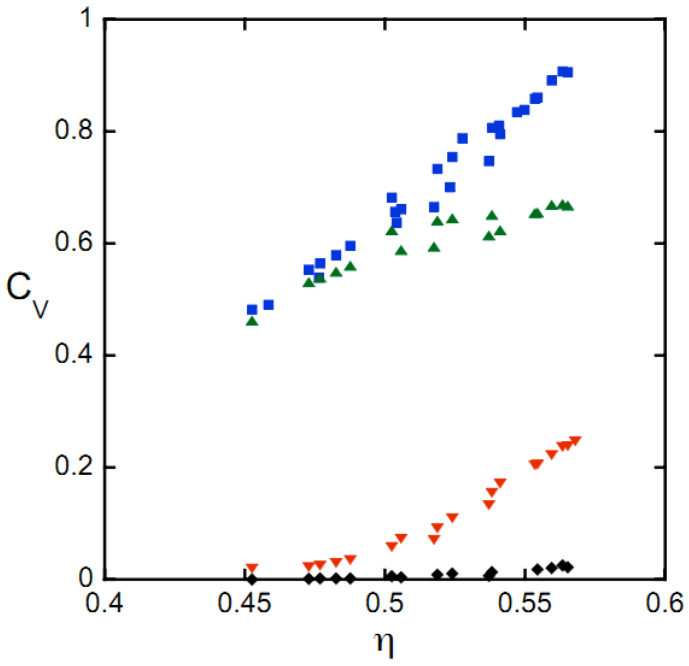

Figure 12. Plot of the nonbonded potential energy contribution to the heat capacity as a function packing fraction. The squares are the full heat capacity, the inverted triangles are the results from the quenching simulations, and the triangles are the difference between the two. The diamonds are the contribution to the heat capacity from the bonds in the quenched simulations.

Additionally, this sheds some light on the (standard thermodynamic) heat capacity, which is the low frequency limit of the dynamic heat capacity (see Fig. 12). A large increase in the heat capacity as the glass transition is approached (at high packing fractions), is seen to be due to the configurational (i.e. IS) contribution to the heat capacity. (This up tick in the heat capacity near the glass transition is seen in experiment as well; see e.g. Fig 6 of [47]). The increase in relaxation times as the glass transition is approached correlates with an increasing contribution of

the IS to the heat capacity. For such packing fractions the system is being constrained by the PEL. Whereas, for low packing fractions, there is no notable α-peak contribution from the configurational heat capacity, meaning the IS are not playing an important part in the dynamics of the system.

So far, the quenching has been done for 23 attractive FR systems and 11 attractive FJ systems. Although this has not been done for every system simulated, it does cover the range of packing fractions used in the other simulations.

A paper on this topic covering our methodology and the results presented here has been published in JCP [48] and has been selected for publication in the Virtual Journal of Biological Physics Research (volume 21, issue 11).

3.4. Nonlinear Dynamic Heat Capacity

3.4.1. Background

In nonlinear studies an addition independent variable is introduced: the (nontrivial) amplitude of the perturbation of the system, which in the case of our dynamic heat capacity study is the amplitude of the temperature wave ΔT. Nonlinear relaxation studies have been done both in the time domain and the frequency domain. In the time domain, a large sudden change to the system one direction is differentiated from a jump in the other direction. For example, suddenly dropping the temperature of a system by a large amount causes a slower relaxation than suddenly raising it [49] (see Fig 13).

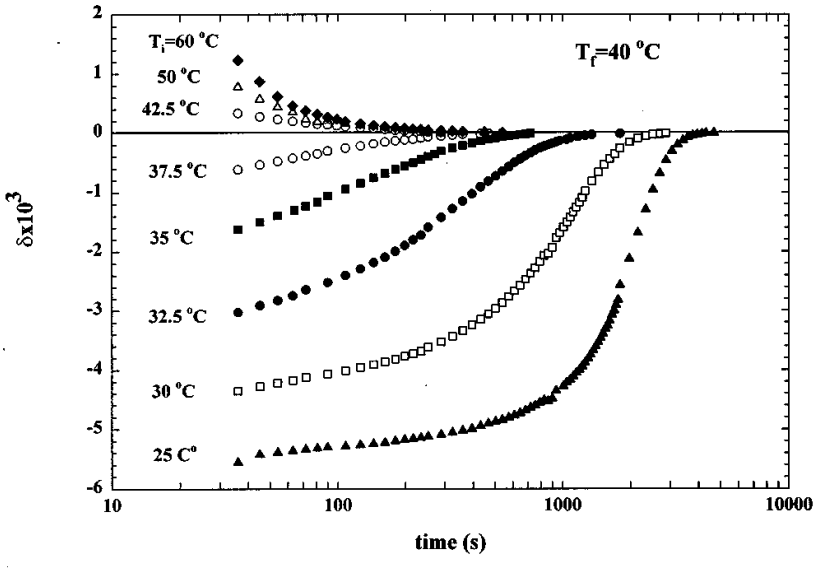

Figure 13. Volume recovery for poly(vinyl acetate) subjected to a temperature jump from T_i to T_f. The large jump in the temperature produces nonlinear results: note the asymmetry of the relaxation function between the upward and downward jumps in temperature. This is figure 3 from [49].

In the frequency domain, the most common application for nonlinear studies is large amplitude oscillatory shear (LAOS) experiments [50, 51]. In short, a piece of material in question is placed under a sinusoidal shear strain with variable amplitude and frequency; as the amplitude of the strain is increased, the assumptions of linear response theory no longer hold. The analysis for such experiments is done using a Fourier series. Once the system has reached steady state, the shear stress response to the input strain will be periodic, but not necessarily sinusoidal. Such a function can always be written as a Fourier series:

$$f(t) = a_0 + \sum_{n=1}^{\infty}\left[a_n \cos(n\omega t) + b_n \sin(n\omega t)\right] \tag{13}$$

where a_0 is the DC response of the system, a_1 and b_1 become the loss and storage in the low amplitude limit, and a_n and b_n (n>1) are the higher harmonics. In the case of LAOS, a_0=0, and provided there is not and slip between the apparatus and the material, a_{2k}=b_{2k}=0 for any k (both of these facts are due to the fact that the system is symmetric across the midpoint of the oscillation without slip) [50, 51]. Additionally, the in phase components b_n, n odd, are similar to the storage and the out of phase components a_n, n odd, play a similar role to the loss.

Another tool that is also used in this field are Lissajous-Bowditch plots, where the input wave and output wave (e.g. shear and stress in LAOS, or temperature and energy in dynamic heat capacity) are plotted against each other [50, 51]. The degree of nonlinearity is easily shown by such plots because, if the system were linear, these plots would be ellipses, and nonlinear behavior shows up as deformities in these elliptical shapes.

3.4.2. Methodology and Results

We ran nonlinear oscillatory simulations with the quenching procedure of the previous section at a fixed state point (T=2.0, ρ=1.06, FR) with a variety of amplitude temperatures. Example Lissajous-Bowditch-like plots of these simulations with frequencies near the α and β peaks are shown in Fig. 14. Note that, unlike the LAOS example above, large amplitude dynamic heat capacity systems are not symmetric about the midpoint of oscillation, which is the expected result: the energy response to low temperature should not mirror the energy response to high temperature. This asymmetry (the presence of even term in the Fourier series) is analogous to the asymmetry across the δ=0 line in Fig. 13.

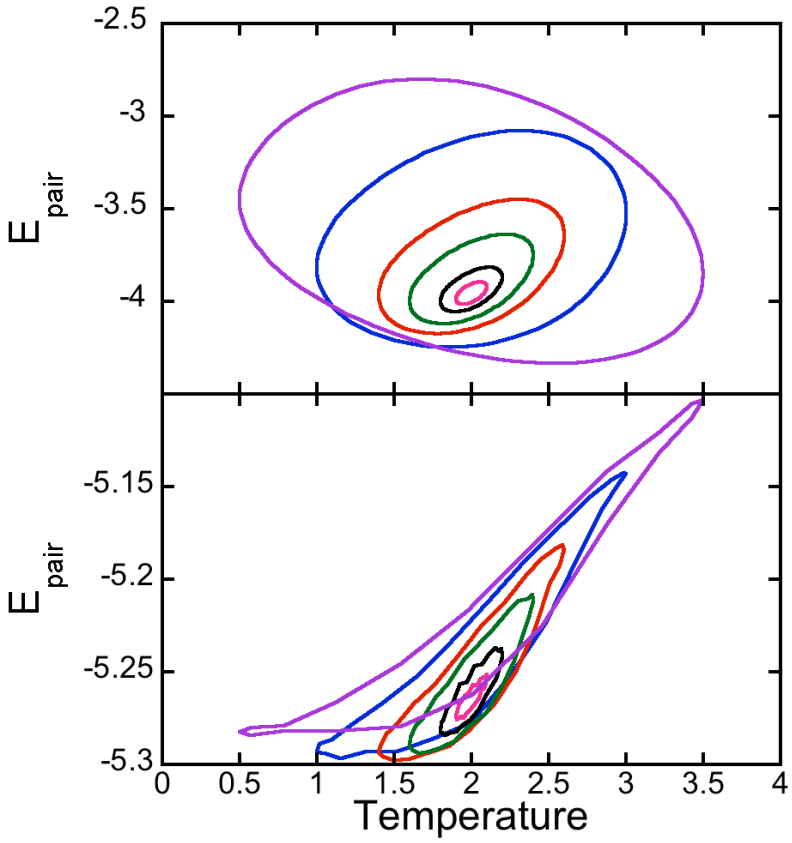

Figure 14. Parametric plots of the pairwise energy against temperature (averaged over several periods) for a frequency near the β-peak (top), and a frequency near the α-peak (bottom). The bottom plot is quenched energy and the top plot is the unquenched energy.

In addition to the Fourier series analysis discussed above, we can also define something similar to a nonlinear storage and loss. Particularly, plugging equation (10) into the formula for entropy generation per cycle (6), we can separate the Fourier terms into "entropy preserving" ones (analogous to the in phase component and the storage) and "entropy generating" ones (similar to the out of phase component and the loss). Skipping the details of the integral, it can be shown that

$$S_{gen/cycle} = -\frac{1}{T_0}\frac{2\pi}{\sqrt{1-\alpha^2}}\sum_{n=1}^{\infty}(-\gamma)^n n\begin{cases}(-1)^k a_n, & n=2k-1\\ (-1)^k b_n, & n=2k\end{cases} \tag{14}$$

where $\alpha = \Delta T/T_0$, and $\gamma = (1/\alpha)[1-(1-\alpha^2)^{1/2}]$. As $\alpha \to 0$, this approaches the result of equation (6). Thus, we can define a nonlinear thermodynamic loss as

$$Loss = \frac{S_{gen/cyc}}{\pi\alpha^2} \tag{15}$$

which collapses into the imaginary part of the dynamic heat capacity as ΔT gets small. Notice that, because of the asymmetry with respect to high and low temperature, that we have contributions from even terms in the series of equation (11). Also, we can interpret the loss-like terms in the sequence as the odd *a* terms and the even *b* terms, i.e. the "out of phase" contributions of the odd harmonics and the "in phase" contributions of the even harmonics.

To generalize the storage as well, we note that in the linear response regime the root mean squared of the signal is proportional to the absolute value of the transfer function (in this case heat capacity) at that frequency. To preserve this relationship, we define the nonlinear storage as

$$Storage = \sqrt{2\left(\frac{rms}{\Delta T}\right)^2 - \left(\frac{S_{gen/cyc}}{\pi\alpha^2}\right)^2} \tag{16}$$

where the root mean square of a Fourier series (ignoring the constant component) is given by Parseval's theorem:

$$rms^2 = \frac{1}{2}\sum_{n=1}^{\infty}\left(a_n^2 + b_n^2\right) \tag{17}$$

For the system studied, the quenched nonlinear storage and loss are shown in Fig. 15. Notice that as the amplitude of the temperature wave is increased, the peak in the loss becomes broader and shifted to higher frequencies. So, the nonlinear response is accessing a broader range of relaxation times, but the overall relaxation time is decreasing. Although, due to computational limitations, we were not able to actually see it, in the low frequency limit one expects that the storage should approach the standard linear heat capacity, as the loss term dies off to zero.

A paper on the methods and results presented in this section is in progress.

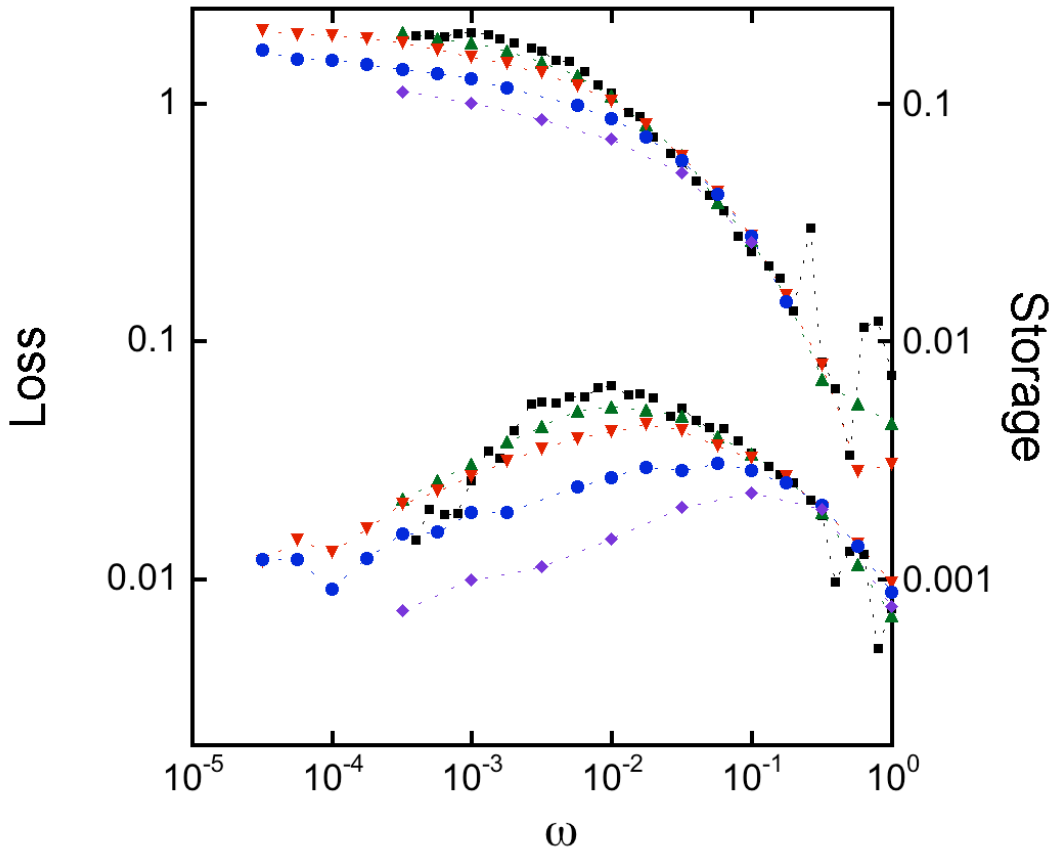

Figure 15. Plot of the nonlinear storage (top curves, right scale) and loss (bottom curves, left scale) on a log-log scale. Note that the right and laft scale are offset by an order of magnitude, for clarity. The squares are the linear approximation, $\Delta T=0.1T_0$. The triangles are $\Delta T=0.2T_0$. The inverted triangles are $\Delta T=0.3T_0$. The circles are $\Delta T=0.5T_0$. The diamonds are $\Delta T=0.75T_0$.

5. SUMMARY AND CONCLUSIONS

The first main result of the work is based on Monte Carlo simulations of the east Ising model; we can compute the dynamic heat capacity of the model and fit it to relaxation functions to extract relaxation time and form. The relaxation time is seen to fit the general form that it should from theoretical arguments from the literature. Secondly, we make a connection between the rules of the east model and its structure (domains of down spins with up spin on either side) to a Markov chain model of those domains to get a discrete set of relaxation times. These relaxation times explain the shape of the dynamic specific heat spectra at low temperature and high frequency. A full description of the dynamics would require us to model the domain-domain interactions. Such a model would speed up the relaxation times based on the (probabilistic) size of the domain to the left. This would result in a gradual isolated/nonisolated domain transition, where timescales near the relaxation time of the median domain size would dominate the long time behavior. However, the simple fix presented to account for the nonisolated dynamics introduces only a single fitting parameter, but fits the dynamics very well.

In a broader sense, the whole purpose of the east model is to replicate a real system. For a remarkable number of real systems and experiments, we see relaxations that for at least certain timescales appears to be stretched exponential. For these functions to be exactly correct, this would require that there was a continuous distribution of relaxation times in the system; a claim that is not necessarily physical. Discrete models, such as the east model, also show relaxation behavior that, for certain timescales at least, is very similar to the KWW form, but since they are discrete we do not need to invoke a continuous distribution of relaxation times to generate them. It is not such a huge leap to suppose that a similar mechanism is at work in real systems as well. That is, certain jammed structures have certain (temperature dependent) times associated with them and the sum of all their relaxations give rise to the macro level experimental results. What exactly these are, and how they evolve with time is a much more complicated question.

The primary results for the dynamic heat capacity simulations on the bead-spring polymeric model (Section 3), are the replication of experiment in our simulations: the low frequency relaxation behavior (the α-peak) observed in simulation is similar to what is seen in experiment and approximately follows a Cole-Davidson form, and the collapse of the dynamical data to packing fraction that was present in previous studies on this same system was preserved.

Adding quenching to the dynamic heat capacity simulations resulted in the (expected, yet important) result that the low frequency part of the response function (the α-peak) is almost entirely due to motion between inherent structures of the potential energy landscape. That is, the piece of the response function that can be observed in experiment is due entirely to an inherent structural contribution. Therefore building models for the PEL might be a sufficient explanation of long time behaviors of glassy materials.

Finally, by relating the “loss” term of the dynamic heat capacity to the entropy generation per cycle of the oscillatory simulation (or experiment), we can formulate a generalized response function for nonlinear experiments based on thermodynamically meaningful terms. For our

system, the highly nonlinear dynamics were “spread out” over a wider distribution of relaxation times compared to the linear system.

6. REFERENCES

[1] Debenedetti, P.G. & Stillinger, F.H. Supercooled liquids and the glass transition. *Nature* **410**, 259-267 (2001).

[2] Kauzmann, W. The Nature of the Glassy State and the Behavior of Liquids at Low Temperatures. *Chemical Reviews* **43**, 219-256 (1948).

[3] Angell, C.A., Ngai, K.L., McKenna, G.B., McMillan, P.F. & Martin, S.W. Relaxation in glassforming liquids and amorphous solids. *J. Appl. Phys.* **88**, 3113-3157 (2000).

[4] Kohlrausch, F. Bemerkungen zu Hrn. Neesen's Beobachtungen über die elastische Nachwirkung. *Annalen der Physik* **231**, 579–587 (1875).

[5] Kohlrausch, F. Experimental-Untersuchungen über die elastische Nachwirkung bei der Torsion, Ausdehnung und Biegung. *Annalen der Physik* **234**, 337–375 (1876).

[6] Kohlrausch, R. Theorie des elektrischen Rueckstandes in der Leidner Flasche. *Annalen der Physik* **91**, 56-82,179-213 (1854).

[7] Williams, G. & Watts, D.C. Non-symmetrical dielectric relaxation behaviour arising from a simple empirical decay function. *Trans. Faraday Soc.* **66**, 80-85 (1970).

[8] Callen, H.B. & Welton, T.A. Irreversibility and Generalized Noise. *Phys. Rev.* **83**, 34 (1951).

[9] Lindsey, C.P. & Patterson, G.D. Detailed comparison of the Williams--Watts and Cole--Davidson functions. *J. Chem. Phys.* **73**, 3348-3357 (1980).

[10] Nielsen, J.K. & Dyre, J.C. Fluctuation-dissipation theorem for frequency-dependent specific heat. *Phys. Rev. B* **54**, 15754 (1996).

[11] Davidson, D.W. & Cole, R.H. Dielectric Relaxation in Glycerol, Propylene Glycol, and n-Propanol. *The Journal of Chemical Physics* **19**, 1484-1490 (1951).

[12] Birge, N.O. & Nagel, S.R. Specific-Heat Spectroscopy of the Glass Transition. *Phys. Rev. Lett.* **54**, 2674 (1985).

[13] Christensen, T. The Frequency Dependence of the Specific Heat at the Glass Transition. *J. Phys. Colloques* **46**, C8-635-C8-637 (1985).

[14] Brown, J.R., McCoy, J.D. & Adolf, D.B. Driven simulations of the dynamic heat capacity. *The Journal of Chemical Physics* **131**, 104507 (2009).

[15] Garden, J.-L., Richard, J. & Guillou, H. Temperature of systems out of thermodynamic equilibrium. *J. Chem. Phys.* **129**, 044508 (2008).

[16] Ising, E. Beitrag zur Theorie des Ferromagnetismus. *Zeitschrift für Physik A Hadrons and Nuclei* **31**, 253-258 (1925).

[17] Onsager, L. Crystal Statistics. I. A Two-Dimensional Model with an Order-Disorder Transition. *Phys. Rev.* **65**, 117 (1944).

[18] Fredrickson, G.H. & Andersen, H.C. Kinetic Ising Model of the Glass Transition. *Phys. Rev. Lett.* **53**, 1244 (1984).

[19] Fredrickson, G.H. & Andersen, H.C. Facilitated kinetic Ising models and the glass transition. *J. Chem. Phys.* **83**, 5822-5831 (1985).

[20] Palmer, R.G., Stein, D.L., Abrahams, E. & Anderson, P.W. Models of Hierarchically Constrained Dynamics for Glassy Relaxation. *Phys. Rev. Lett.* **53**, 958 (1984).

[21] Jäckle, J. & Eisinger, S. A hierarchically constrained kinetic Ising model. *Zeitschrift für Physik B Condensed Matter* **84**, 115-124 (1991).

[22] Evans, M.R. Anomalous coarsening and glassy dynamics. *Journal of Physics: Condensed Matter* **14**, 1397-1422 (2002).

[23] Aldous, D. & Diaconis, P. The Asymmetric One-Dimensional Constrained Ising Model: Rigorous Results. *Journal of Statistical Physics* **107**, 945-975 (2002).

[24] Cancrini, N., Martinelli, F., Roberto, C. & Toninelli, C. Kinetically constrained spin models. *Probability Theory and Related Fields* **140**, 459-504 (2008).

[25] Brown, J.R., McCoy, J.D. & Borchers, B. Theory and simulation of the dynamic heat capacity of the east Ising model. *J. Chem. Phys.* **133**, 064508 (2010).

[26] Sollich, P. & Evans, M.R. Glassy Time-Scale Divergence and Anomalous Coarsening in a Kinetically Constrained Spin Chain. *Phys. Rev. Lett.* **83**, 3238 (1999).

[27] Grinstead, C.M. & Snell, J.L. *Introduction to Probability*. (American Mathematical Society: 2003).

[28] Plimpton, S. Fast Parallel Algorithms for Short-Range Molecular Dynamics. *Journal of Computational Physics* **117**, 1-19 (1995).

[29] Budzien, J. Computer Simulation Study of the Glass Transition in Chain Molecules Using a Scalar Metric Approach. (2004).

[30] Heffernan, J.V. et al. Rotational relaxation in simple chain models. *J. Chem. Phys.* **127**, 214902-10 (2007).

[31] Budzien, J., McCoy, J.D. & Adolf, D.B. General relationships between the mobility of a chain fluid and various computed scalar metrics. *J. Chem. Phys.* **121**, 10291-10298 (2004).

[32] Dotson, T.C. et al. Rheological complexity in simple chain models. *J. Chem. Phys.* **128**, 184905-9 (2008).

[33] Heffernan, J.V. et al. Molecular flexibility effects upon liquid dynamics. *J. Chem. Phys.* **126**, 184904-9 (2007).

[34] Dotson, T.C., Budzien, J., McCoy, J.D. & Adolf, D.B. Cole-Davidson dynamics of simple chain models. *J. Chem. Phys.* **130**, 024903-9 (2009).

[35] Lennard-Jones, J.E. Cohesion. *Proceedings of the Physical Society* **43**, 461-482 (1931).

[36] Weeks, J.D., Chandler, D. & Andersen, H.C. Role of Repulsive Forces in Determining the Equilibrium Structure of Simple Liquids. *J. Chem. Phys.* **54**, 5237-5247 (1971).

[37] Kremer, K., Grest, G.S. & Carmesin, I. Crossover from Rouse to Reptation Dynamics: A Molecular-Dynamics Simulation. *Phys. Rev. Lett.* **61**, 566 (1988).

[38] Grest, G.S. & Kremer, K. Molecular dynamics simulation for polymers in the presence of a heat bath. *Phys. Rev. A* **33**, 3628 (1986).

[39] Kremer, K. & Grest, G.S. Dynamics of entangled linear polymer melts: A molecular-dynamics simulation. *J. Chem. Phys.* **92**, 5057-5086 (1990).

[40] Stillinger, F. & Weber, T. Hidden structure in liquids. *Phys. Rev. A* **25**, 978-989 (1982).

[41] Schrøder, T.B., Sastry, S., Dyre, J.C. & Glotzer, S.C. Crossover to potential energy landscape dominated dynamics in a model glass-forming liquid. *J. Chem. Phys.* **112**, 9834-9840 (2000).

[42] Yang, Y. & Chakraborty, B. Dynamics in the metabasin space of a Lennard-Jones glass former: Connectivity and transition rates. *Phys. Rev. E* **80**, 011501 (2009).

[43] Doliwa, B. & Heuer, A. Energy barriers and activated dynamics in a supercooled Lennard-Jones liquid. *Physical Review E* **67**, 31506 (2003).

[44] Doliwa, B. & Heuer, A. Hopping in a supercooled Lennard-Jones liquid: Metabasins, waiting time distribution, and diffusion. *Physical Review E* **67**, 30501 (2003).

[45] Carmi, S., Havlin, S., Song, C., Wang, K. & Makse, H.A. Energy-landscape network approach to the glass transition. *Journal of Physics A: Mathematical and Theoretical* **42**, 105101 (2009).

[46] Doye, J.P.K. Network Topology of a Potential Energy Landscape: A Static Scale-Free Network. *Phys. Rev. Lett.* **88**, 238701 (2002).

[47] Efremov, M.Y., Olson, E.A., Zhang, M., Zhang, Z. & Allen, L.H. Probing glass transition of ultrathin polymer films at a time scale of seconds using fast differential scanning calorimetry. *Macromolecules* **37**, 4607–4616 (2004).

[48] Brown, J.R. & McCoy, J.D. The potential energy landscape contribution to the dynamic heat capacity. *J. Chem. Phys.* **134**, 194503 (2011).

[49] Simon, S.L. & McKenna, G.B. Interpretation of the dynamic heat capacity observed in glass-forming liquids. *J. Chem. Phys.* **107**, 8678-8685 (1997).

[50] Cho, K.S., Hyun, K., Ahn, K.H. & Lee, S.J. A geometrical interpretation of large amplitude oscillatory shear response. *J. Rheol.* **49**, 747 (2005).

[51] Ewoldt, R.H. & McKinley, G.H. On secondary loops in LAOS via self-intersection of Lissajous–Bowditch curves. *Rheol Acta* **49**, 213-219 (2009).

DISTRIBUTION

1	MS0359	D. Chavez, LDRD Office, 1911 (electronic copy)
1	MS0899	RIM-Reports Management, 9532 (electronic copy)


Sandia National Laboratories